

INCOMMENSURATE SOLID MONOLAYER OF ^3He ADSORBED ON GRAFOIL:
GENERALIZED HEISENBERG MODEL WITH EXCHANGE FREQUENCIES
EVALUATED BY PATH INTEGRAL TECHNIQUES

B. Bernu[†], D. Ceperley[‡], C. Lhuillier[†] and L. Pierre[†]

[†]Laboratoire de Physique Théorique des liquides.
U.P.M.C., Boite 121, 75252 Paris Cedex 05, France
équipe associée au CNRS

[‡]National Center for Supercomputer Applications
Dept. of Physics, University of Illinois at Urbana-Champaign
1110 W. Green. St., Champaign, IL 61820

ABSTRACT

Recent experiments on ^3He adsorbed on grafoil have shown a very rich phase diagram: commensurate and incommensurate solid phases, coexistence of first solid layers with liquid second or third layers. We focus here on the study of one incommensurate solid layer, for densities between 0.08 and 0.1 atom/ \AA^2 , at temperatures less than 1K. The solid forms a triangular lattice and its Debye temperature is between 20K and 30K. Below 1K, the phonons vanish and the physics is governed only by multiple spin exchanges: the full hamiltonian can be mapped on to a generalized Heisenberg model.

Up to now, experimental data have been analyzed using approximate solutions of the Heisenberg model with an effective pair exchange energy J : however measurements of the specific heat lead to values of J different from those extracted from magnetic susceptibility measurements. In order to go beyond these approximations, we compute *ab initio* various exchange frequencies (2, 3 and 4 body exchanges) at two densities by path integral techniques by evaluating the probability of tunneling from one configuration to its permuted one. These exchange frequencies are then introduced in a generalized Heisenberg model for which we calculate the full spectrum for small periodic systems and derive the thermodynamics.

INTRODUCTION

Helium 3 adsorbed on surfaces presents a large variety of phases depending on the area density and on the strength of the attractive potential with the substrate. The potential between an helium atom and the graphite is very attractive; its depth falls down to -200K . On the contrary, it varies smoothly with the x, y coordinates, with an amplitude of the order of 10K . At low coverage, ^3He is well described as a two-dimensional

Fermi liquid. The solid phase begins for a density larger than $\rho = 0.041 \text{ atom/\AA}^2$. First, the adsorbed helium atoms sit on the minimum of the potential surface to give a commensurate phase. Then for densities greater than 0.07 atom/\AA^2 , the system evolves to an incommensurate phase[1, 2]. For densities larger than 0.11 atom/\AA^2 , the second layer is promoted, which leads in the second layer to a similar scenario as the coverage increases: first, it is a Fermi liquid, then a commensurate solid phase, and finally an incommensurate solid phase.

Here, we focus on the study of an incommensurate solid monolayer, and hence neglect the x, y -dependence of the interaction potential between helium atoms and the substrate. We believe that, in this phase, the corrugation effects are weak. Including them would complicate considerably the calculations. Then, in the incommensurate solid phase, and without the corrugation, the helium atoms form a triangular lattice. The lower collective density-density excitations are the phonons whose energy scale is the Debye temperature θ_D , which is of the order of 20 K, and whose contributions to the specific heat C_V vanish as $(T/\theta_D)^2$. The picture of this system is that helium atoms vibrate randomly in their local ground state. As the temperature decreases, the DeBroglie wavelength increases and very rarely, as the random zero point motions of atoms permit, a few helium atoms permute their position and therefore their spin. These spin exchanges (P) break down the degeneracy of the distinguishable particle ground state into a spectrum of 2^N states, whose energy scale is now given the exchange frequencies J_P , which are in the range of μK to mK . The physics is therefore well described with a generalized Heisenberg hamiltonian for triangular lattice in two dimensions. The sign of the effective pair exchange fixes the ferro or antiferromagnetic character of the system. For dense solids, the cyclic triple exchange is the largest exchange, which leads to a ferromagnetic phase, whereas for less dense solids the two body and the cyclic four body exchanges become comparable to the cyclic triple exchange, which may lead to an antiferromagnetic phase. A possible ferro/antiferromagnetic transition is then possible in the first or in the second layer¹.

Specific heat[2] and magnetization[3] measurements are now available as functions of the coverage and the temperature. Effective pair exchanges are evaluated from these two kinds of experiments, but lead to somewhat different values. Among the possible explanations one can propose: the importance of other multiple exchanges which can lead to different temperature dependencies, the role of defects or the presence of vacancies which would imply more complex effective hamiltonian.

We assume that the lattice is perfect and evaluate its "exact" thermodynamical properties. Exchange frequencies are computed with path integral techniques and, in a second step, the generalized Heisenberg model is solved for small periodic clusters. For simplicity, we focus on the first layer.

THE MODEL

First, we check if our potential model recovers thermodynamical experimental data: solid phase and Debye temperature. The hamiltonian is written down as:

$$H_{\text{layer}} = H_{\text{bulk}} + \sum_i V_S(z_i) \quad (1)$$

where z_i is the distance from the surface, H_{bulk} is the hamiltonian for bulk helium, where we use the Aziz potential[4]. V_S is the potential between an helium atom and the surface of graphite. This potential is fitted to reproduce the excitation spectrum of one

¹Because the J 's vary very rapidly with the density and the layer, we can assume in a first approximation that the first and the second layers are uncoupled.

atom at

where V_S is the potential between an helium atom and the surface of graphite.

The corrugation of the potential surface leads to a transition from a Fermi liquid to a solid phase.

where ρ_0 is the density of the solid phase. The exact value of the transition density stands for this trial wave function. The error is shown in figure 1 a. In the solid phase, the one body excitation is greater than the two body excitation, which determines the magnetic character of the solid phase.

²Corrugation of the potential surface leads to a transition from a Fermi liquid to a solid phase. In our case.

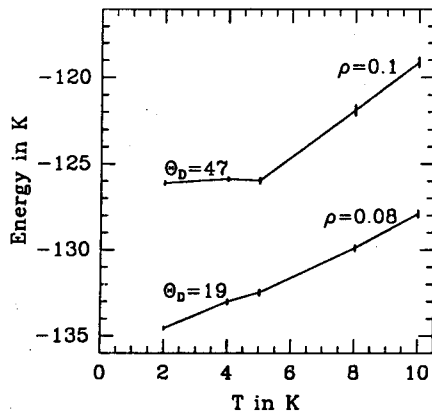


Figure 1: Energy versus temperature for a ^3He monolayer .

atom at the surface:

$$V_S(z) = V_0 \exp(-z/z_s) - C_3/(z - z_0) \quad (2)$$

where $V_0 = 3.7 \cdot 10^6$, $z_s = 0.281$, $C_3 = 2130$ and $z_0 = 1$, the distances are expressed in angstroms and energies in Kelvin. Its depth is about -200K .

The thermodynamical properties are evaluated from path integral techniques, using an analytical expression for the approximate many-body density matrix at high temperature:

$$\rho_T(R, R'; \tau) = \prod_{i=1}^N \rho_0(r_i, r'_i; \tau) \exp(u_i^s(z_i, z'_i; \tau)) \prod_{1 \leq i < j \leq N} \exp(u_{ij}^b(r_{ij}, r'_{ij}; \tau)) \quad (3)$$

where ρ_0 is the free particle density matrix, $\exp(u^s)$ is the contribution of the exact density matrix of one helium at the surface of the grafoil and $\exp(u^b)$ is the contribution the exact density matrix of two isolated helium atoms². In Eq. 3, $R \equiv \{r_1, \dots, r_N\}$ stands for $3N$ -dimensional vectors and r for 3-dimensional vectors. The correction to this trial density matrix is evaluated by calculating $\partial \rho / \partial \tau - H_{\text{layer}} \rho$ [5]. We believe that the error on the energy due to this approximate density matrix is less than 0.5K . In figure 1 are reported the total energies for the two densities 0.08 and 0.1 atom per \AA^2 . In the simulations, we check the stability of the solid phase by computing the average one body density. The density plots show a tendency for melting at temperatures greater than 5K in agreement with experimental results[6]. The Debye temperature is determined by fitting the energy at the lowest temperatures using[2, 7]:

$$E(T) = E(T=0) + \frac{28.848}{3} \frac{T^3}{\Theta^2} \quad (4)$$

²Corrugation would lead to a 6-dimensional potential tabulation of u^s instead of a 2-dimensional in our case .

At the lowest density the Debye temperature is close to the experimental evaluation of 20K, and the variations with the density agree with a ρ^3 dependence[8].

The one body density profile $n(z)$ is very close to $\Psi_0^2(z)$, where Ψ_0 is the ground state of an helium atom in the external potential $V_S(z)$. $n(z)$ does not depend on the density, but as the temperature increases some particles jump to the second layer and one can see a second maximum around the equilibrium position of a second layer. It is important to notice that the second excited state of the one body problem has an energy 60K above the ground state[9].

PATH INTEGRAL EVALUATION OF EXCHANGE FREQUENCIES

We evaluate the exchange frequencies with the same method as was used in solid ^3He by Ceperley et al.[10]. The equilibrium lattice sites are denoted by $Z = \{z_1, z_2, \dots, z_N\}$, and a permutation by P . If the barriers between the $N!$ equilibrium positions PZ are infinite, all configurations have the same energy. This degeneracy is broken by the exchange of atoms.

Permutations are very rare and occur roughly every 10^5 atomic vibrations. So it is not practical to wait for the system to jump by itself from one configuration to another. But this property allows us to focus on one permutation at a time.

To define the exchange frequency J_P associated to a permutation P , we assume that the ground state is split into two states ϕ_0 and ϕ_1 with even and odd symmetry, and energies E_0 and E_1 . If the system is localized around Z (resp. PZ), it is described by $\Psi_Z = \phi_0 + \phi_1$ ($\Psi_{PZ} = \phi_0 - \phi_1$). It oscillates from Z to PZ at the frequency $\hbar\omega_P = E_1 - E_0 = 2J_P$.

For solid ^3He , it is the repulsive part of the potential and not the Fermi statistics, which creates a cage effect, restricting the motion in the phase space around Z . Therefore the density matrix around an equilibrium position Z or PZ is given by the distinguishable particle density matrix:

$$\rho(R, R'; \beta) = \sum_n e^{-\beta E_n} \phi_n(R) \phi_n(R')$$

and for the unpermuted and permuted reference positions, we have:

$$\begin{aligned} \rho(Z, Z; \beta) &\sim e^{-\beta E_0} [\phi_0^2(Z) + e^{-\beta(E_1-E_0)} \phi_1^2(Z)] \\ \rho(Z, PZ; \beta) &\sim e^{-\beta E_0} [\phi_0(Z) \phi_0(PZ) + e^{-\beta(E_1-E_0)} \phi_1(Z) \phi_1(PZ)] \end{aligned}$$

From the ratio of these two matrix elements, we deduce:

$$F_P(\beta) = \frac{\rho(Z, PZ; \beta)}{\rho(Z, Z; \beta)} = \tanh(J_P(\beta - \beta_P)) \quad (5)$$

where $J_P \beta_P = \ln \{\phi_1^2(Z) / \phi_0^2(Z)\}$.

Inserting (M-1) intermediate points R_1, R_2, \dots, R_{M-1} into Eq. 5 we convert it into a path integral:

$$F_P(\beta) = \frac{\int dR_1 dR_2 \dots dR_{M-1} \rho(Z, R_1; \tau) \dots \rho(R_{M-1}, PZ; \tau)}{\int dR_1 dR_2 \dots dR_{M-1} \rho(Z, R_1; \tau) \dots \rho(R_{M-1}, Z; \tau)} \quad (6)$$

with $\tau = \beta/M$. If M is large enough, an accurate expression for $\rho(R, R'; \tau)$ can be written down, and we use Eq. 3.

Since
close to
of Eq. 6
written

where we
introduc
variables
new varia
The point
a time $k\tau$
try to ma
of Eq. 11.
permutat
permutat
of R'_{i+1}, \dots
Comp
The reason
mutation
 R_i and R
by splitting
second on
tries to m
spent in t

The ad
techniques
frequency,
eigenvalue

The fo
with $M =$
in the first
the additi
specially f

Since the potential between helium atoms is hard-core like, most of the points R_i are close to either Z or PZ . This means that only a few points of the path in the numerator of Eq. 6 go from Z to PZ . This picture implies that the numerator of Eq. 6 can be written as:

$$\rho(Z, PZ, \beta) = \int dR_1 dR_2 \dots dR_{M-1} \rho(Z, R_1; \tau) \dots \rho(R_{M-1}, PZ; \tau) \quad (7)$$

$$= \int dR_i dR_{i+k} \rho(Z, R_i; i\tau) \rho(R_i, PR_{i+k}; k\tau) \rho(PR_{i+k}, PZ; (M-k-i)\tau) \quad (8)$$

$$= \int dR_i dR_{i+k} \rho(Z, R_i; i\tau) \rho(R_i, PR_{i+k}; k\tau) \rho(R_{i+k}, Z; (M-k-i)\tau) \quad (9)$$

$$= \int dR_1 \dots dR_i dR'_{i+1} \dots dR'_{i+k-1} dR_{i+k} \dots dR_{M-1} \\ \times \rho(Z, R_1; \tau) \dots \rho(R_{i-1}, R_i; \tau) \\ \times \rho(R_i, R'_{i+1}; \tau) \dots \rho(R'_{i+k-1}, PR_{i+k}; \tau) \\ \times \rho(R_{i+k}, R_{i+k+1}; \tau) \dots \rho(R_{M-1}, Z; \tau) \quad (10)$$

$$= \int dR_1 \dots dR_i dR_{i+1} \dots dR_{i+k-1} dR_{i+k} \dots dR_{M-1} \\ \times \rho(Z, R_1; \tau) \dots \rho(R_{M-1}, Z; \tau) \\ \times \frac{\int dR'_{i+1} \dots dR'_{i+k-1} \rho(R_i, R'_{i+1}; \tau) \dots \rho(R'_{i+k-1}, PR_{i+k}; \tau)}{\rho(R_i, R_{i+1}; \tau) \dots \rho(R_{i+k-1}, R_{i+k}; \tau)} \quad (11)$$







where we use $\rho(PR, PR'; \tau) = \rho(R, R'; \tau)$ to go from Eq. 8 to Eq. 9. Eq. 10 is found by introducing again elementary paths with the time step τ and by labeling R' the dummy variables for the exchange part of the path. The last step is obtained by introducing new variables $R_{i+1} \dots R_{i+k-1}$ and multiplying and dividing by the corresponding ρ 's. The points R are near Z , and the points R' form a path which goes from R_i to PR_{i+k} in a time $k\tau$. This means that during an equilibrium walk of distinguishable particles, we try to map a path between R_i and PR_{i+k} . $F_P(\beta)$ is then the mean value of the last line of Eq. 11. For a given path $\{R_1, \dots, R_{M-1}\}$, we choose all initial positions R_i and try all permutations P' equivalent to P (for example, all first neighbors pair permutations): the permutation P' fixes the end point of the partial path at $P'R_{i+k}$. Then the multisampling of $R'_{i+1}, \dots, R'_{i+k-1}$ is done and the histogram of path contribution ratio is accumulated.

Computed directly by this algorithm, the convergence of the method will be poor. The reason is, that during an equilibrium configuration only the points close to Z (permutation identity) are sampled and there is a small probability of finding configurations R_i and R_{i+k} so that $\rho(R_i, PR_{i+k}; \tau)$ is not small. Much faster convergence is achieved by splitting this computation in two parts: the first one is described above and in the second one evaluate the inverse of Eq. 5: starting from a permuted configuration, one tries to map on to unpermuted configurations. Optimization of the computational time spent in these two parts is done as in classical statistical mechanics by Bennett[11].

The advantage of this method combining classical statistical mechanics and quantum techniques is that the convergence is independent of the magnitude of J_P , the tunneling frequency, since we evaluate the ratio of two probabilities and not the differences between eigenvalues.

The following exchange frequencies have been obtained from simulations at $T = 1K$, with $M = 40$ and $k = 4$. We do not find a ferromagnetic/antiferromagnetic transition in the first layer. The comparison with a pure 2D model (see the table I) shows that the additional motions of atoms in the z -direction enhance the exchange frequencies, specially for high densities and for the two and four body exchanges.

Table 1. Exchange frequencies in μK . ρ is in $\text{atom}/\text{\AA}^2$. α is fitted from $J_P \sim \rho^{-\alpha}$. J_{eff} is defined by Eq. 16. The upper box is the 3D simulation with the substrate potential, while the lower box corresponds to pure 2D exchange frequencies.

3D	$\rho = .0785$	$\rho = .09$	$\rho = .1$	α
	29 ± 2	1.3 ± 0.2	0.157 ± 0.014	22
	48 ± 5	3.5 ± 0.3	0.33 ± 0.03	21
	25 ± 4	0.78 ± 0.14	0.066 ± 0.009	25
J_{eff}	36	4	0.34	19
2D	$\rho = .081$	$\rho = .105$		
	4.6 ± 0.6	0.0026 ± 0.0003		29
	28 ± 2	0.024 ± 0.002		27
	2.6 ± 0.2	0.00055 ± 0.00005		33
J_{eff}	45	0.044		26

GENERALIZED HEISENBERG MODEL, COMPARISONS WITH EXPERIMENTS

Here, we evaluate the thermodynamical properties for the generalized Heisenberg model, where the hamiltonian is defined by:

$$H = - \sum_P (-1)^P J_P P \quad (12)$$

where the summation includes all cyclic permutations involving up to four nearest neighbor particles and P is the spin permutation operator (for a transposition $P_{ij} = 1/2 + 2\vec{S}_i \cdot \vec{S}_j$). The system is an infinite periodic triangular lattice where the separation between two neighbors is $a = \sqrt{2/\rho\sqrt{3}}$. On this lattice, we superpose a lattice of diamond cells with a side length d (see figure 2), and acute angles of $\pi/3$. The side of a diamond can be any line between two sites and is of the form $l\vec{u} + m\vec{v}$, where \vec{u} and \vec{v} are vectors of length a and with an angle of $\pi/3$. The length d of this vector fixes the number N of atoms in the cell: $N = (d/a)^2 = l^2 + m^2 + lm$. The cases where N is less or equal to 16 have been studied.

The full spectrum of the generalized Heisenberg hamiltonian is calculated by the Lanczos method. The group G of symmetries of the hamiltonian is the direct product

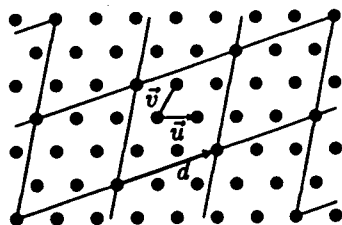
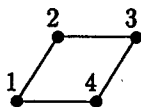


Figure 2. Example of a periodic system: $N = 7$, $l = 2$ and $m = 1$. The diamond side length d is $\sqrt{7}a$, where a is the separations between sites.

$G_s \times G_l$ of the spin symmetry group $G_s (\equiv SU_2)$ and the lattice symmetry group G_l , which contains N translations \times 6 rotations = $6N$ permutations of the sites. Casually, G_l may also contain axial reflexions and then it has $12N$ elements. These symmetries are responsible for the energy degeneracy. Each eigenvalue is associated with an irreducible representation (I.R.) of G which characterizes the symmetry of its eigenvectors. Its multiplicity is equal to the dimension of this irreducible representation. For each relevant I.R., i , the Lanczos method is applied in a space, \mathcal{E}_i , where the degeneracy is removed. Because the dimension d_i of \mathcal{E}_i are small (the maximum is 116 for $N = 16$), the full spectrum may be computed. In fact, we use only the I.R. of the group G_l to reduce the dimensionality. The I.R. of G_s (i.e. the total spin) are taken into account in another way. At each iteration of the Lanczos method, the new vector is projected on the eigen subspace of S^2 under consideration and then orthogonalized to all the previous ones. This last precaution, even if expensive in computational time, is necessary to prevent wrong degeneracies from appearing.

The general hamiltonian involving up to four body exchanges is written from the hamiltonian of one diamond. Labeling particles as follows:



the most general hamiltonian for a diamond involves 8 different types of permutations:

$$\begin{aligned} -H_D = & -J_{11}[P_{12} + P_{23} + P_{14} + P_{24} + P_{34}] - J_{13}P_{13} \\ & + K_{111}[P_{124} + P_{142} + P_{234} + P_{243}] \\ & + K_{113}[P_{123} + P_{132} + P_{134} + P_{143}] \\ & - L_{1111}[P_{1234} + P_{1432}] \\ & - L_{1113}[P_{1243} + P_{1342} + P_{1423} + P_{1324}] \\ & + L'_{1111}[P_{12}P_{34} + P_{14}P_{32}] + L'_{1113}P_{13}P_{24} \end{aligned}$$

All cyclic permutations are then grouped using the properties for cyclic permutations [12, 13]:

$$\begin{aligned} P_{123} + P_{132} &= P_{12}P_{13} + P_{13}P_{12} = P_{12} + P_{23} + P_{13} - 1 \\ P_{1234} + P_{1432} &= P_{12}P_{13}P_{14} + P_{14}P_{13}P_{12} \\ &= -1 + P_{13} + P_{24} + P_{12}P_{34} + P_{14}P_{23} - P_{13}P_{24}. \end{aligned}$$

and when summing over all diamonds, one finally gets:

$$\begin{aligned} H = & \sum_{\langle 11 \rangle} \tilde{J}_{11}P_{ij} + \sum_{\langle 13 \rangle} \tilde{J}_{13}P_{ij} \\ & + \sum_{\langle 1111 \rangle} \tilde{J}_{1111}P_{ij}P_{kl} + \sum_{\langle 1113 \rangle} \tilde{J}_{1113}P_{ij}P_{kl} + CN \end{aligned} \quad (13)$$

where $\langle 11 \rangle$ means first neighbors and $\langle 13 \rangle$ means second neighbors (1-3 means a distance of $\sqrt{3}a$) and the \tilde{J} 's are defined as:

$$\begin{aligned} \tilde{J}_{11} &= J_{11} - 2K_{111} - 4K_{113} + L_{1111} + 4L_{1113} \\ \tilde{J}_{13} &= J_{13} - 2K_{113} + L_{1111} \\ \tilde{J}_{1111} &= -L'_{1111} + L_{1111} \\ \tilde{J}_{1113} &= -L'_{1113} - L_{1111} + 2L_{1113} \\ C &= 2K_{111} + 6K_{113} - 3L_{1111} - 6L_{1113} \end{aligned} \quad (14)$$

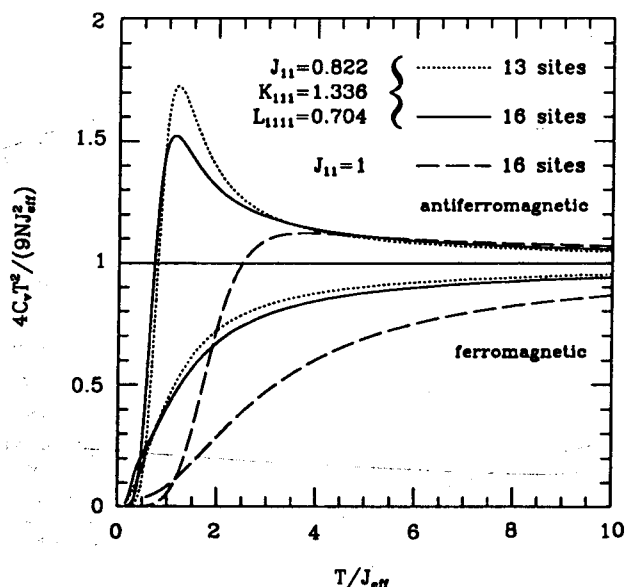


Figure 3. Deviations of C_V from its high temperature limit (Eq. 15) for two different sets of exchange frequencies. Down (up) is the (anti)ferromagnetic case.

Note that with these definitions, the \tilde{J} 's are not necessarily positive. The phase diagram for this hamiltonian depends only on four independent parameters[14]. The specific heat at high temperature for this model is then given by:

$$C_V/(N\beta^2) = \frac{9}{4}J_{\text{eff}}^2 \quad (15)$$

where

$$\begin{aligned} J_{\text{eff}}^2 = & \tilde{J}_{11}^2 + 4\tilde{J}_{11}\tilde{J}_{1111} + \tilde{J}_{11}\tilde{J}_{1113} \\ & + \tilde{J}_{13}^2 + \tilde{J}_{13}\tilde{J}_{1113} \\ & + 6\tilde{J}_{1111}^2 + 3\tilde{J}_{1111}\tilde{J}_{1113} + \frac{5}{4}\tilde{J}_{1113}^2 \end{aligned} \quad (16)$$

When we retain the three most important exchange (J_{11} , K_{111} and L_{1111}) in J_{eff} , we obtain $J_{\text{eff}}^2 = (J_{11} - 2K_{111} + \frac{5}{2}L_{1111})^2 + 2L_{1111}^2$. In table are given the values of J_{eff} for three densities.

On figure 3 are plotted the specific heat deviations from the high temperature limit for the case of a pure Heisenberg model (only pair exchange) and for the case of multi-exchange frequencies (of a ^3He monolayer at the density $0.08 \text{ atom}/\text{\AA}^2$). For comparison the data are scaled with J_{eff} . Important changes in C_V are obtained between these two cases, where the effect are more dramatic in the antiferromagnetic case (reverse all the signs of \tilde{J}).

By comparison with the experiments of Greywall[2], it appears that our values are one order of magnitude smaller than his last evaluations of J_{eff} . Our data seem to be in better agreement with magnetization data[15], even if the complete analysis of this comparison is not yet achieved.

REFER

- [1] D.
- [2] D.
- [3] H.
H.
L.J.
Ca
C.J.
J. S
- [4] R.A.
J. C
- [5] D.M.
Ca
- [6] S.H
- [7] J.G
- [8] S.V.
edit
- [9] F. J
- [10] D.M
- [11] C.H
- [12] D.J.
- [13] M. I
- [14] see a
- [15] H. C

REFERENCES

- [1] D.S. Greywall and P.A. Busch, *Phys. Rev. Lett.* **65** 2788 (1990);
- [2] D.S. Greywall *Phys. Rev. B* **41** 1842 (1990);
- [3] H. Godfrin, R.R. Ruel and D.D. Osheroff, *Phys. Rev. Lett.* **60** 305 (1988);
H. Godfrin, *Can. J. Phys.* **65** 1430 (1987);
L.J. Friedman, S.N. Ytterboe, H.M. Bozier, A.L. Thomson, M.C. Cross,
Can. J. Phys. **65** 1351 (1987);
C.P. Lusher, J. Saunders, B.P. Cowan, *Europhys. Lett.* **14** 809 (1991);
J. Saunders, C.P. Lusher, B.P. Cowan, *Phys. Rev. Lett.* **21** 2523 (1990);
- [4] R.A. Aziz, V.P.S. Nain, J.S. Carley, W.L. Taylor and G.T. McConville,
J. Chem. Phys. **70** 4330 (1979);
- [5] D.M. Ceperley and E. L. Pollock, Proceedings of the Elba Conference on Monte Carlo Methods for Physics, 1990.
- [6] S.H. Hering, S.W. Van Sciver and O.E. Vilches *J. Low Temp. Phys.* **25** 793 (1976);
- [7] J.G. Dash, *Films on Solid Surfaces* Academic, New-York (1975);
- [8] S.V. Hering and O.E. Vilches in *Monolayer and Submonolayer Helium films* edited by J.G. Daunt and E. Lerner (Plenum, New-York, 1973);
- [9] F. Joly, C. Lhuillier, B. Brami submitted to *Surface Sciences*;
- [10] D.M. Ceperley and G. Jacucci, *Phys. Rev. Lett.* **58** 1648 (1987);
- [11] C.H. Bennett *J. Comput. Phys.* **22** 245 (1976);
- [12] D.J. Thouless, *Proc. R. Phys. Soc. London* **86** 893 (1965);
- [13] M. Roger, J.H. Hetherington, and J.M. Delrieu, *Rev. Mod. Phys.* **55** 1 (1983);
- [14] see also for another hamiltonian model : M. Roger, *Phys. Rev. Lett.* **64** 297 (1990);
- [15] H. Godfrin, private communication;